Response to Comments by Review #1

Manuscript: egusphere-2024-2416

Title: Measurement Report: Optical and structural properties of atmospheric water-soluble organic carbon in China: Insights from multi-site spectroscopic measurements

Authors: Haibiao Chen et al.

Corresponding author: Caiqing Yan (email: cyan0325@sdu.edu.cn)

General Comments: *The reviewer appreciates the efforts of authors for collecting a good number samples from ten sites of China, and doing a variety of analyses using absorbance and fluorescence spectrometry as well as FTIR. The data have been plotted properly. However, the interpretations are often hand wavy and lack scientific rigour. It limits the sufficient exploitation of such hard-earned data by the authors.*

The reviewer recommends the major revisions before the manuscript can be considered for publication in the journal ACP.

Response to General Comments: We thank the reviewer for your overall supportive comments. We also appreciate the considerable efforts you put into reviewing the manuscript and providing valuable comments and suggestions for the improvements and clarifications. Based on your comments and suggestions, the manuscript is thoroughly revised. Especially, we have made careful thinking and revisions to interpret the data more rationally, so as to improve the rigor and scientific nature of the discussion.

Below, we detail our responses and resulting edits to all the comments. These are organized such that we first list the review comments in italics and blue, immediately followed by our responses in normal font. To make it clear, the contents in the revised manuscript are presented in quotes and italics, while the newly added contents in the revised manuscript are underlined.

Major comments:

Comment #1: *L51-53: This is a wrong statement. WSOC is a largely variable fraction of aerosols and numerous studies have shown that water-insoluble OC can be more absorbing BrC (Cheng et al., 2016, Atmospheric Environment). A proper literature review must be added here with the clear information on both water-soluble and water-insoluble BrC. Subsequently, add the limitation of this study which used water-soluble BrC only.*

Response to Comment #1: We thank the reviewer for pointing this out and making constructive suggestions. We agree with the reviewer that the statement here (especially that WSOC generally acts as a substitute of BrC) is not

accurate. According to the reviewer's suggestion, we have added a description of water-soluble and water-insoluble BrC in the revised manuscript, and added the limitations that this study only focuses on water-soluble BrC in the conclusion sections. The sentences have been revised as follows,

(1) In the introduction section:

"Solvent-soluble organic carbon (e.g., water-soluble organic carbon, WSOC; methanol-soluble organic carbon, MSOC) is often used to act as a substitute of BrC. In particular, light absorption of WSOC has been extensively studied, due to its widespread presence and high atmospheric abundance in the atmosphere, as well as mature extraction methods, although some previous studies have indicated that water-insoluble OC (WISOC) contains more light-absorbing BrC (Cao et al., 2021; Chen et al., 2024b; Cheng et al., 2016; Yan et al., 2017). Absorption and fluorescence spectroscopy are two of the most widely used methods to reveal optical properties of WSOC (Wang et al., 2022b; Wu et al., 2021). By light-absorption spectroscopy analysis, light absorption characteristics and capabilities of WSOC from different sources or environments are usually characterized by the absorption coefficient or mass absorption efficiency of a specific wavelength over the range of 360-370 nm (average 365 nm) (Hecobian et al., 2010). And the direct radiative forcing of WSOC can be further estimated by simplified radiative forcing models combined with the measured absorption coefficient."

(2) In the conclusion section:

"Additionally, it is important to note that this study only focused on WSOC. Since the WISOC may have stronger light absorption capacity, further research on light absorption, composition and structure of WISOC (especially in northern China in winter) and the correlation between them are also needed in the future."

References:

Cao, T., Li, M., Zou, C., Fan, X., Song, J., Jia, W., Yu, C., Yu, Z., and Peng, P. a.: Chemical composition, optical properties, and oxidative potential of water- and methanol-soluble organic compounds emitted from the combustion of biomass materials and coal, Atmospheric Chemistry and Physics, 21, 13187-13205, https://doi.org/10.5194/acp-21-13187-2021, 2021.

Chen, H., Zhou, R., Fang, L., Sun, H., Yang, Q., Niu, H., Liu, J., Tian, Y., Cui, M., and Yan, C.: Variations in optical properties of water- and methanol-soluble organic carbon in $PM_{2.5}$ in Tianjin and Handan over the wintertime of 2018-2020, Atmospheric Research, 303, 107332, https://doi.org/10.1016/j.atmosres.2024.107332, 2024b.

Cheng, Y., He, K. B., Du, Z. Y., Engling, G., Liu, J. M., Ma, Y. L., Zheng, M., and Weber, R. J.: The characteristics of brown carbon aerosol during winter in Beijing, Atmospheric Environment, 127, 355-364,

https://doi.org/10.1016/j.atmosenv.2015.12.035, 2016.

Yan, C., Zheng, M., Bosch, C., Andersson, A., Desyaterik, Y., Sullivan, A.P., Collett, J.L., Zhao, B., Wang, S.X., He, K.B., Gustafsson, Ö. Important fossil source contribution to brown carbon in Beijing during winter. Scientific Reports, 7, 43182, https://doi.org/10.1038/srep43182, 2017.

Comment #2: *Section 2.1: Briefly provide details of sampler, sampling duration, frequency, total number of samples, etc and then refer Table S1 for details.*

Response to Comment #2: We thank the reviewer's kind reminder and constructive suggestions. We have taken the reviewer's suggestion, added a brief description of the sampling information, and made the following modifications in the revised manuscript,

"$PM_{2.5}$ samples are collected at eight urban sites and two regional sites in China during the late November and January of 2019-2020 (see Figure S1 and Table S1). .... In this study, daytime, nighttime or daily $PM_{2.5}$ samples were collected using medium- or high-volume samplers at different sites with a sampling duration of 11 h-24 h for each sample. More detailed sampling information and sample sizes are summarized in Table S1 in the Supplement. It is worth noting that in this study, the daily average of the parameters measured at each site is used for subsequent summary and comparison."

Comment #3: *L119-120: Give a valid reason for selecting this wavelength range only for AAE calc*

Response to Comment #3: We appreciate the reviewer's kind reminder and apologize for the confusion caused. In this study, the selection of wavelength range was mainly based on the following considerations: (1) to avoid the light absorption interference of inorganic substances (such as ammonium nitrate, sodium nitrate and nitrate ions) at shorter wavelengths (< 250 nm) (Afsana et al., 2022), (2) to ensure that WSOC has a more significant light absorption signal (see the new Figure. 4 in the revised manuscript), and (3) the fitting of the power-law of log Abs_{λ} and log λ used to calculate the AAE values is good (see Figure R1). In view of these above criteria, we re-select the data in the range of 300-500 nm to calculate the AAE values in the revised manuscript.

In the revised manuscript, we have added the reason for selecting the wavelength range for the AAE calculation to the supplementary materials (please see Text S2), and revised the relevant discussion and description of AAE values in the main text and chart accordingly.

"In this study, AAE is fitted over the wavelength range of 300-500 nm in consideration of avoiding the interference

from light-absorbing inorganic compounds (e.g., ammonium nitrate, sodium nitrate and nitrate ions) at shorter wavelengths (< 250 nm) and ensuring significant light absorption signals of WSOC at longer wavelengths (Afsana et al., 2022; Ting et al., 2022; Yan et al., 2015). Moreover, the power-law fit of all samples' absorption coefficients between 300 and 500 nm is good with r^2 > 0.99 (see Figure S2)." (in the Supplement)

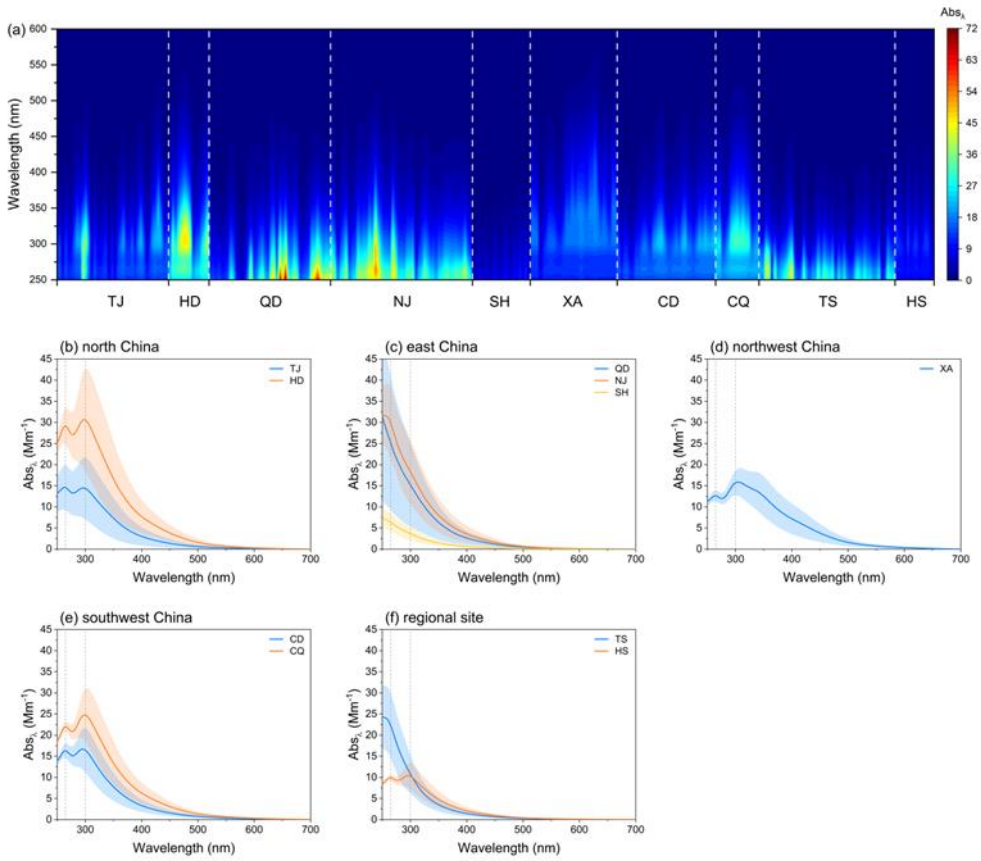

Figure 4. *(a) Light absorption coefficient spectrum of WSOC at each site and the average light absorption spectrum in (b) north China, (c) east China, (d) northwest China, (e) southwest China, and (f) regional sites. Note: The color bar represents the magnitude of the* Abs_{λ}.

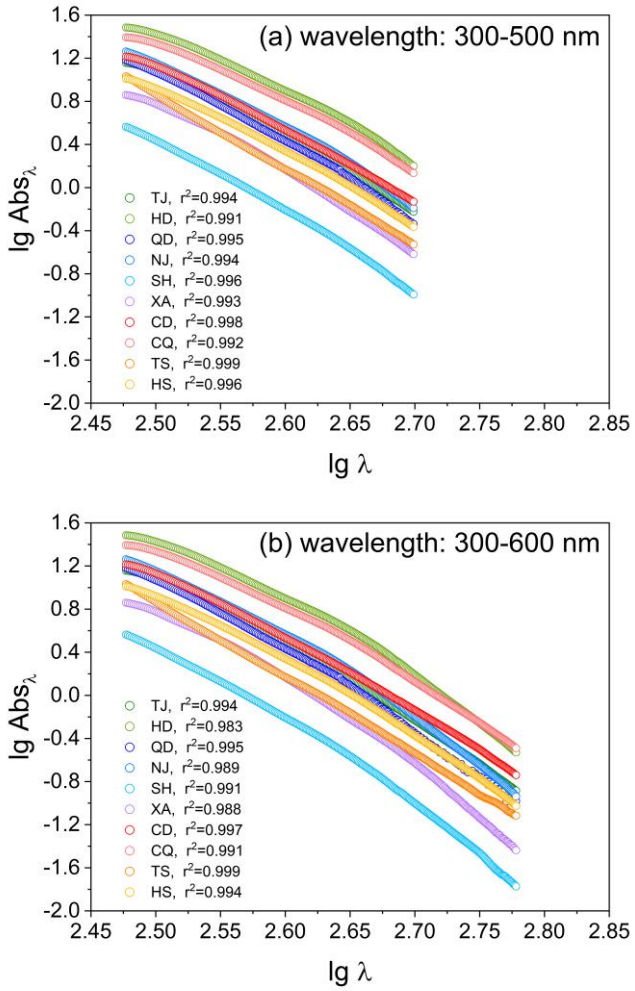

Figure R1. Comparison of power-law fitting curves for light absorption in different wavelength ranges: (a) 300-500 nm and (b) 300-600 nm.

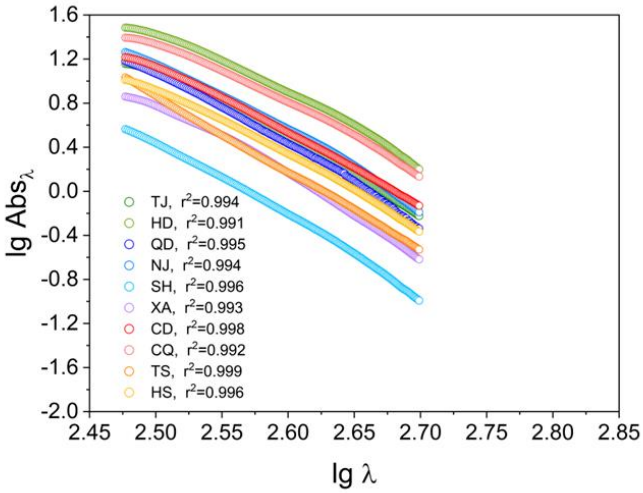

Figure S2. *The power-law fitting curves of light absorption in the wavelength range of 300-500 nm.*

References:

Afsana, S., Zhou, R., Miyazaki, Y., Tachibana, E., Deshmukh, D. K., Kawamura, K., and Mochida, M.: Abundance,

chemical structure, and light absorption properties of humic-like substances (HULIS) and other organic fractions of forest aerosols in Hokkaido, Sci Rep, 12, 14379, https://doi.org/10.1038/s41598-022-18201-z, 2022.

Ting, Y.-C., Ko, Y.-R., Huang, C.-H., Cheng, Y.-H., and Huang, C.-H.: Optical properties and potential sources of water-soluble and methanol-soluble organic aerosols in Taipei, Taiwan, Atmospheric Environment, 290, 119364, https://doi.org/10.1016/j.atmosenv.2022.119364, 2022.

Yan, C. Q., Zheng, M., Sullivan, A. P., Bosch, C., Desyaterik, Y., Andersson, A., Li, X. Y., Guo, X. S., Zhou, T., Gustafsson, O., and Collett, J. L.: Chemical characteristics and light-absorbing property of water-soluble organic carbon in Beijing: Biomass burning contributions, Atmospheric Environment, 121, 4-12, https://doi.org/10.1016/j.atmosenv.2015.05.005, 2015.

Comment #4: *L165-170: This is very hand wavy discussion. Statement shall be substantiated by logical arguments and supporting data.*

Response to Comment #4: We agree with the reviewer that the statement should be substantiated by logical arguments and supporting data. To make the discussion here more reasonable, we used Hybrid Single-Particle Lagrangian Integrated Trajectory (HYSPLIT) model to analyze the 48-h backward air mass trajectories that arriving at the ten sites to assess the impact of anthropogenic and oceanic emissions. And this statement has been revised as follows,

"Moreover, concentrations of carbonaceous components in inland cities (i.e., HD, NJ, XA, CD, CQ) are much higher than those in coastal cities (i.e., TJ, QD, SH) ($p < 0.01$), which is consistent with that reported in previous studies that have shown that air masses from the ocean generally contain lower levels of aerosol content and carbonaceous components (Chen et al., 2023; Diesch et al., 2012; Mo et al., 2022; Zhang et al., 2022b). The 48-h backward air mass trajectory analysis shows that about 1/5 to 1/2 of the air masses that arrive at the coastal cities during the observation period pass through the ocean region, while the inland cities are predominately affected by continental air masses, which may contain a large number of anthropogenic aerosols (see Figure S4). Furthermore, it is worth noting that the regional site TS in NCP has a relatively low mass concentration of carbonaceous components compared to urban sites, which may be due to its high altitude (~1500 m) and low local anthropogenic activities (Jiang et al., 2020). In contrast, the mass concentrations of carbonaceous components at HS (another regional site) in the PRD region are relatively higher compared to TS site. The backward air mass trajectory analysis indicates that more than 80% of the air masses arriving at the HS site originated from the PRD region and are accompanied by low wind speeds (1.54 $m \cdot s^{-1}$ on average during the sampling period). This suggests that

there may be high anthropogenic emissions in the PRD region during the winter sampling period."

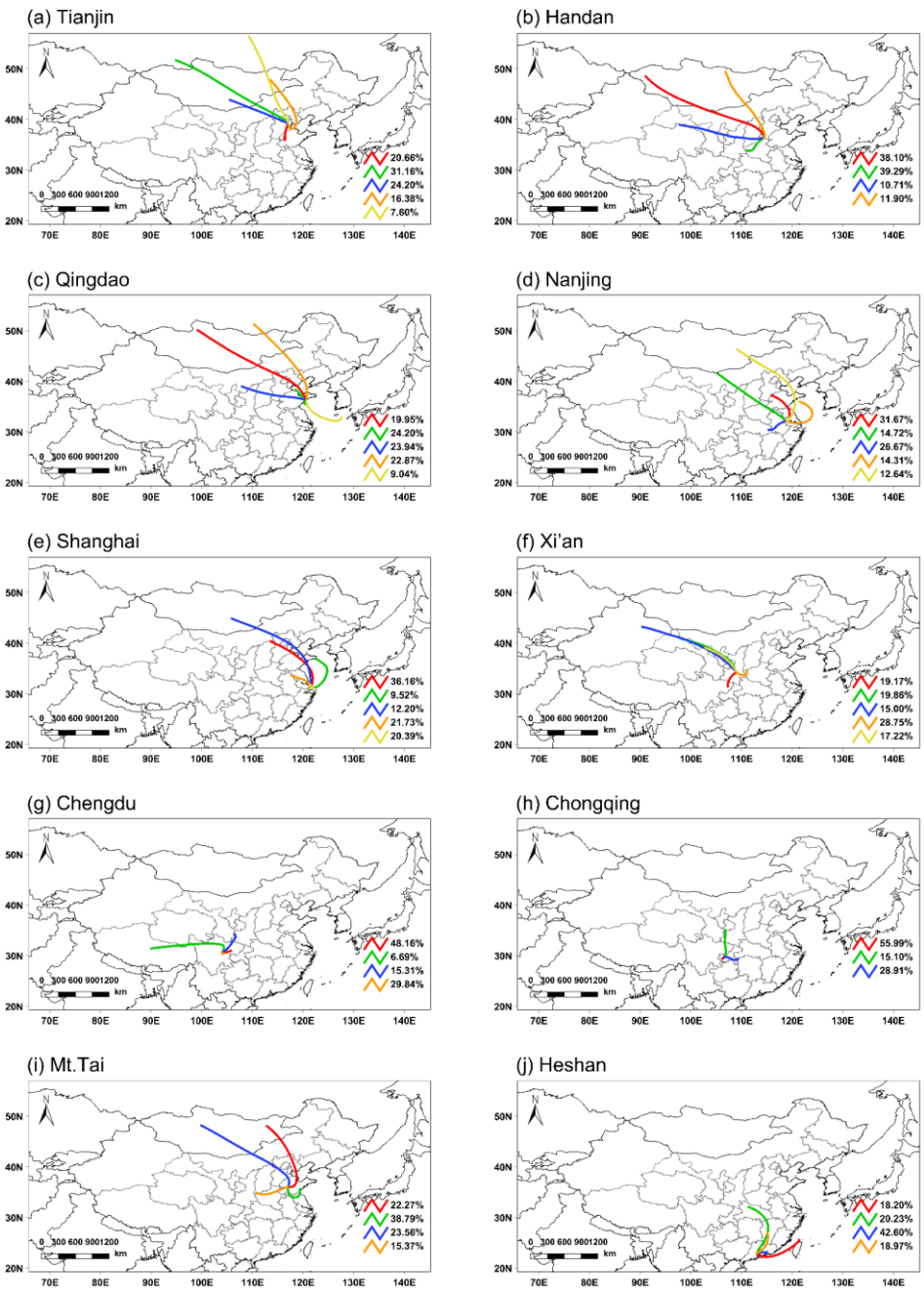

Figure S4. *Clusters of air masses derived from backward trajectory analysis at the ten sites. The 48-h backward trajectories at each site are calculated every 1 h and clustered at an ending height of 500 m above ground level based on the MeteoInfoMap software.*

References:

Chen, H., Yan, C., Fu, Q., Wang, X., Tang, J., Jiang, B., Sun, H., Luan, T., Yang, Q., Zhao, Q., Li, J., Zhang, G., Zheng, M., Zhou, X., Chen, B., Du, L., Zhou, R., Zhou, T., and Xue, L.: Optical properties and molecular composition of wintertime atmospheric water-soluble organic carbon in different coastal cities of eastern China,

Science of the Total Environment, 892, 164702, https://doi.org/10.1016/j.scitotenv.2023.164702, 2023.

Diesch, J. M., Drewnick, F., Zorn, S. R., von der Weiden-Reinmüller, S. L., Martinez, M., and Borrmann, S.: Variability of aerosol, gaseous pollutants and meteorological characteristics associated with changes in air mass origin at the SW Atlantic coast of Iberia, Atmospheric Chemistry and Physics, 12, 3761-3782, https://doi.org/10.5194/acp-12-3761-2012, 2012.

Jiang, Y., Xue, L., Gu, R., Jia, M., Zhang, Y., Wen, L., Zheng, P., Chen, T., Li, H., Shan, Y., Zhao, Y., Guo, Z., Bi, Y., Liu, H., Ding, A., Zhang, Q., and Wang, W.: Sources of nitrous acid (HONO) in the upper boundary layer and lower free troposphere of the North China Plain: Insights from the Mount Tai Observatory, Atmospheric Chemistry and Physics, 20, 12115-12131, https://doi.org/10.5194/acp-20-12115-2020, 2020.

Mo, Y. Z., Zhong, G. C., Li, J., Liu, X., Jiang, H. X., Tang, J., Jiang, B., Liao, Y. H., Cheng, Z. N., and Zhang, G.: The sources, molecular compositions, and light absorption properties of water-soluble organic carbon in marine aerosols from South China Sea to the Eastern Indian Ocean, Journal of Geophysical Research: Atmospheres, 127, https://doi.org/10.1029/2021JD036168, 2022.

Zhang, J., Qi, A., Wang, Q., Huang, Q., Yao, S., Li, J., Yu, H., and Yang, L.: Characteristics of water-soluble organic carbon (WSOC) in $PM_{2.5}$ in inland and coastal cities, China, Atmos. Pollut. Res., 13, 101447, https://doi.org/10.1016/j.apr.2022.101447, 2022b.

Comment #5: *L190-191: This discussion should also consider the effects of meteorological processes on Abs_{365} e.g., photo-bleaching or photo-enhancement.*

Response to Comment #5: We agree with the reviewer that atmospheric processes, including meteorological processes, also have an impact on Abs_{365}. To make it more accurate, we have made the following modifications,

"This spatial variation may be related to the diversity of WSOC sources and can be affected by the atmospheric processes (including meteorological processes), and is intrinsically related to the chemical composition and structures of WSOC at different sites (Wang et al., 2023; Wang et al., 2024). Previous studies have indicated that the increase in primary emissions such as coal combustion and biomass burning during the winter heating period in Northern China will lead to an enhancement of the WSOC light absorption (Yan et al., 2017; Zhang et al., 2021). The strong correlation between Abs_{365} and POC (r range: 0.59-0.90) or SOC (r range: 0.43-0.97) ($p < 0.01$) (see Figure S6) indicates that light-absorbing components in WSOC are simultaneously affected by both primary emission and secondary formation. The effects of different factors such as chemical composition/structure, and

meteorological conditions on the light absorption of WSOC will be discussed in detail in the following sections."

References:

Wang, D., Shen, Z., Yang, X., Huang, S., Luo, Y., Bai, G., and Cao, J.: Insight into the Role of NH_3/NH_4^+ and NO_x/NO_3^- in the Formation of Nitrogen-Containing Brown Carbon in Chinese Megacities, Environmental Science & Technology, https://doi.org/10.1021/acs.est.3c10374, 2024.

Wang, Y., Feng, Z., Yuan, Q., Shang, D., Fang, Y., Guo, S., Wu, Z., Zhang, C., Gao, Y., Yao, X., Gao, H., and Hu, M.: Environmental factors driving the formation of water-soluble organic aerosols: A comparative study under contrasting atmospheric conditions, Science of The Total Environment, 866, https://doi.org/10.1016/j.scitotenv.2022.161364, 2023.

Yan, C., Zheng, M., Bosch, C., Andersson, A., Desyaterik, Y., Sullivan, A.P., Collett, J.L., Zhao, B., Wang, S.X., He, K.B., Gustafsson, Ö. Important fossil source contribution to brown carbon in Beijing during winter. Scientific Reports, 7, 43182. https://doi.org/10.1038/srep43182, 2017.

Comment #6: *L198-204: These statements shall be endorsed by some source apportionment studies which reported biomass/residential heating as major source over these regions.*

Response to Comment #6: We thank the reviewer's constructive suggestion. We take the reviewer's suggestion and have supplemented the statements as follows,

"Figure 1 illustrates the $\log_{10}(MAE_{405})$ and $AAE_{300\text{-}500}$ values of WSOC measured in this study and reported in previous studies. The map in $\log_{10}(MAE_{405})$ vs. $AAE_{300\text{-}500}$ space has been proposed by Saleh (2020) to classify BrC types based on light-absorbing properties. Notably, most values measured at the ten sites in this study fall in the regions of weakly-absorbing BrC (W-BrC), which are similar to the values of ambient samples reported in previous studies. However, there are slight differences in the distribution of values between each site. QD has the widest range of $\log_{10}(MAE_{405})$ and $AAE_{300\text{-}500}$ values, and is also close to the values of biomass burning samples. Previous studies have indicated that biomass burning (especially those related to residential heating and cooking activities) around the sampling site in QD in winter is a major source contributor to atmospheric particulate matter (Li et al., 2024), and has a significant impact on the light absorption of WSOC (Zhan et al., 2022a; Zhan et al., 2022b). The difference in light absorption of WSOC generated from different fuel (e.g., corn straw, rice straw and pine branch) combustion may be the reason for the wide range of $\log_{10}(MAE_{405})$ and $AAE_{300\text{-}500}$ values in QD (Fan et al., 2016). The values in SH are much closer to very weakly-absorbing BrC (VW-BrC) compared to other sites, which may be

related to the influence of marine air mass, as the backward air mass trajectory analysis shows that more than half of the air masses arriving in SH passing through the ocean area during the sampling period (see Figure S4). In contrast, the values in XA are mainly distributed in the moderately-absorbing BrC (M-BrC) region, with a few samples falling in the W-BrC region. This indicates that WSOC in XA has a stronger light-absorbing capacity, which is consistent with its higher Abs_{365} and MAE_{365} values. The average value in XA is much closer to that of coal combustion source samples. Previous studies conducted in XA have shown that the light-absorbing capacity of WSOC in XA region is always at a high level, especially during the winter heating period when anthropogenic emissions such as biomass burning and coal combustion activities increased (Huang et al., 2018; Lei et al., 2019; Yuan et al., 2020). The cause of the high light absorption level of WSOC in XA needs to be further investigated."

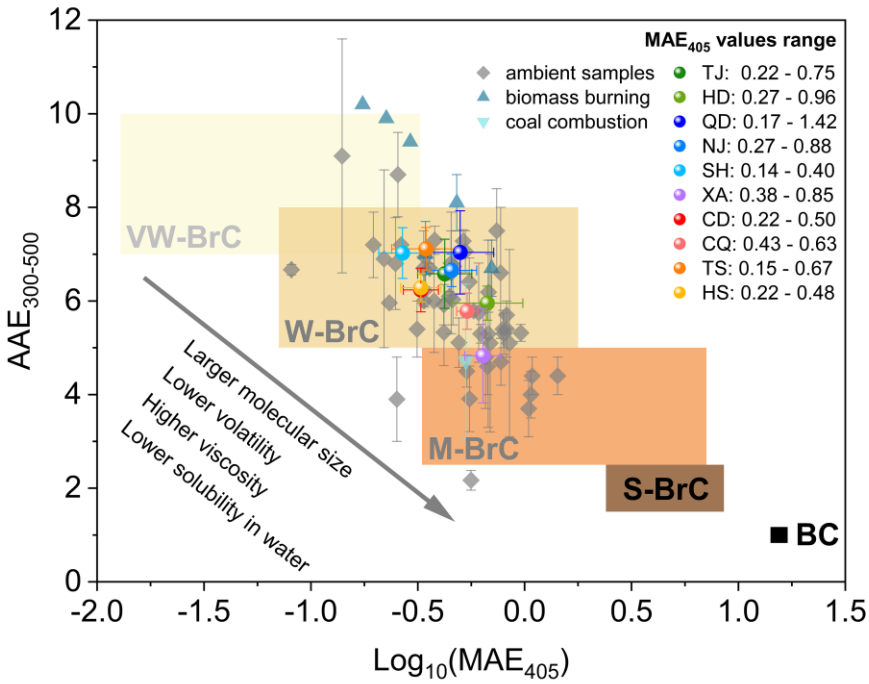

Figure 1. *Graphical representation of optical-based BrC classes in $log_{10}(MAE_{405})$-AAE space. The shaded regions represent very weakly light-absorbing BrC (VW-BrC), weakly light-absorbing BrC (W-BrC), moderately light-absorbing BrC (M-BrC), strongly light-absorbing BrC (S-BrC), and absorbing BC, respectively.*

References:

Fan, X. J., Wei, S. Y., Zhu, M. B., Song, J. Z., and Peng, P. A.: Comprehensive characterization of humic-like substances in smoke $PM_{2.5}$ emitted from the combustion of biomass materials and fossil fuels, Atmospheric Chemistry and Physics, 16, 13321-13340, https://doi.org/10.5194/acp-16-13321-2016, 2016.

Huang, R. J., Yang, L., Cao, J., Chen, Y., Chen, Q., Li, Y., Duan, J., Zhu, C., Dai, W., Wang, K., Lin, C., Ni, H.,

Corbin, J. C., Wu, Y., Zhang, R., Tie, X., Hoffmann, T., O'Dowd, C., and Dusek, U.: Brown carbon aerosol in urban Xi'an, northwest China: The composition and light absorption properties, Environmental Science & Technology, 52, 6825-6833, https://doi.org/10.1021/acs.est.8b02386, 2018.

Lei, Y., Shen, Z., Zhang, T., Lu, D., Zeng, Y., Zhang, Q., Xu, H., Bei, N., Wang, X., and Cao, J.: High time resolution observation of $PM_{2.5}$ Brown carbon over Xi'an in northwestern China: Seasonal variation and source apportionment, Chemosphere, 237, 124530, https://doi.org/10.1016/j.chemosphere.2019.124530, 2019.

Li, R.Y., Yan, C.Q., Meng, Q.P., Yue, Y., Jiang, W., Yang, L.X., Zhu, Y.J., Xue, L.K., Gao, S.P., Liu, W.J., Chen, T.X., Meng, J.J. Key toxic components and sources affecting oxidative potential of atmospheric particulate matter using interpretable machine learning: Insights from fog episodes. Journal of Hazardous Materials, 465, 133175, https://doi.org/10.1016/j.jhazmat.2023.133175, 2024.

Saleh, R.: From measurements to models: Toward accurate representation of brown carbon in climate calculations, Current Pollution Reports, 6, 90-104, https://doi.org/10.1007/s40726-020-00139-3, 2020.

Yuan, W., Huang, R. J., Yang, L., Guo, J., Chen, Z. Y., Duan, J., Wang, T., Ni, H. Y., Han, Y. M. M., Li, Y. J., Chen, Q., Chen, Y., Hoffmann, T., and O'Dowd, C.: Characterization of the light-absorbing properties, chromophore composition and sources of brown carbon aerosol in Xi'an, northwestern China, Atmospheric Chemistry and Physics, 20, 5129-5144, https://doi.org/10.5194/acp-20-5129-2020, 2020.

Zhan, Y., Tsona, N. T., Li, J., Chen, Q., and Du, L.: Water-soluble matter in $PM_{2.5}$ in a coastal city over China: Chemical components, optical properties, and source analysis, journal of Environmental Sciences, 114, 21-36, https://doi.org/10.1016/j.jes.2021.07.011, 2022a.

Zhan, Y., Li, J., Tsona, N. T., Chen, B., Yan, C., George, C., and Du, L.: Seasonal variation of water-soluble brown carbon in Qingdao, China: impacts from marine and terrestrial emissions, Environmental Research, 212, 113144, https://doi.org/10.1016/j.envres.2022.113144, 2022b.

Comment #7: *L210-214: How? Add possible mechanism.*

Response to Comment #7: We thank the reviewer's good question. We have made relevant speculations and supplements, and the revisions are as follows,

"It should be noted that $SFE_{300-400}$ accounts for more than 40% (38.6 ± 5.04%-48.9 ± 4.05% on average) of $SFE_{300-700}$ across the ten sites in this study, which is consistent with a previous study (Deng et al., 2022), indicating that the light absorption of WSOC plays a crucial role in the aerosol direct radiative forcing in the UV-Vis range.

Notably, there is a significant negative correlation ($p < 0.01$) between SFE value and WSOC/OC at most sites (see Figure S7c and d). The WSOC/OC ratio has been used to infer the degree of secondary aerosol formation or aging of aerosols (Dasari et al., 2019; Ram et al., 2012), therefore, the reduction of SFE value of WSOC may be related to the secondary or aged organic aerosols. Previous studies have indicated that the light absorption capacity of secondary BrC is usually lower than that of primary BrC (Fan et al., 2018; Tang et al., 2020; Zhong and Jang, 2011). Furthermore, BrC chromophores with aromatic rings and nitro and phenolic groups may undergo photolysis or photochemical oxidation under sunlight, resulting in photo-bleaching and decrease of light absorption capacity and radiation effect of WSOC (Dasari et al., 2019). However, it is noted that this is only a speculation, and further research is needed in the future in conjunction with atmospheric chemical processes and WSOC component analysis."

References:

Dasari, S., Andersson, A., Bikkina, S., Holmstrand, H., Budhavant, K., Satheesh, S., Asmi, E., Kesti, J., Backman, J., Salam, A., Bisht, D. S., Tiwari, S., Hameed, Z., and Gustafsson, O.: Photochemical degradation affects the light absorption of water-soluble brown carbon in the South Asian outflow, Science Advances, 5, eaau8066, https://doi.org/10.1126/sciadv.aau8066, 2019.

Fan, X., Li, M., Cao, T., Cheng, C., Li, F., Xie, Y., Wei, S., Song, J., and Peng, P. a.: Optical properties and oxidative potential of water-and alkaline-soluble brown carbon in smoke particles emitted from laboratory simulated biomass burning, Atmospheric Environment, 194, 48-57, https://doi.org/10.1016/j.atmosenv.2018.09.025, 2018.

Ram, K., Sarin, M. M., and Tripathi, S. N.: Temporal trends in atmospheric $PM_{2.5}$, PM_{10}, elemental carbon, organic carbon, water-soluble organic carbon, and optical properties: Impact of biomass burning emissions in the Indo-Gangetic Plain, Environmental Science & Technology, 46, 686-695, https://doi.org/10.1021/es202857w, 2012.

Tang, J., Li, J., Su, T., Han, Y., Mo, Y. Z., Jiang, H. X., Cui, M., Jiang, B., Chen, Y. J., Tang, J. H., Song, J. Z., Peng, P. A., and Zhang, G.: Molecular compositions and optical properties of dissolved brown carbon in biomass burning, coal combustion, and vehicle emission aerosols illuminated by excitation-emission matrix spectroscopy and Fourier transform ion cyclotron resonance mass spectrometry analysis, Atmospheric Chemistry and Physics, 20, 2513-2532, https://doi.org/10.5194/acp-20-2513-2020, 2020.

Zhong, M. and Jang, M.: Light absorption coefficient measurement of SOA using a UV–Visible spectrometer connected with an integrating sphere, Atmospheric Environment, 45, 4263-4271, https://doi.org/10.1016/j.atmosenv.2011.04.082, 2011.

Comment #8: *L249-254: The discussion is mostly data description. Author shall attempt to extract science and more substance out of it.*

Response to Comment #8: We thank the reviewer for pointing out this problem and putting forward constructive suggestions. We have reanalyzed these data and made the following changes in the revised manuscript,

"Figure 2 illustrates the average fluorescence volume (FV) and relative contributions of different fluorophores at different sites. Clearly, the average FV of all fluorophores varies in the range of 2.50×10^2-9.76×10^3 RU-nm^2, showing great spatial variability. Overall, the LO-HULIS fluorophore has the highest FV ($1.49\times10^3 \pm 4.74\times10^2$-$9.76\times10^3 \pm 5.82\times10^3$ RU-nm^2 on average) and accounts for the largest proportion (42.2 ± 5.59%-60.3 ± 2.11% on average) in the total fluorophores at most sites (except for TS, NJ and CD), demonstrating the widespread existence of combustion-related sources (especially biomass burning) and their important influence on the fluorophore. In contrast, HO-HULIS fluorophore accounts for the lowest proportion (12.5 ± 1.32%-23.8 ± 2.43% on average, except for TJ and TS). This suggests that the effect of secondary anthropogenic sources at different location may be relatively small during the winter study period. The relatively high FV values of LO-HULIS and non-Nas in northern cities (1.62×10^6 RU-nm^2 in total) compared to southern cities (4.37×10^5 RU-nm^2 in total) and regionals sites (1.76×10^5 RU-nm^2 in total) further indicate the impact of increased primary emissions during the heating season, especially in northern China (Cao et al., 2023; Li et al., 2023b). This is consistent with a previous study by Cao et al., (2024a), which showed that the FV of fluorophores in BrC during the winter heating season was significantly higher than that during the non-heating season."

References:

Cao, J., Shang, J., Kuang, Y., Jiang, X., Shi, X., and Qiu, X.: Molecular composition of Beijing $PM_{2.5}$ Brown carbon associated with fluorescence revealed by gas chromatography time-of-flight mass spectrometry and parallel factor analysis, Atmospheric Environment, 333, https://doi.org/10.1016/j.atmosenv.2024.120670, 2024a.

Cao, T., Li, M., Xu, C., Song, J., Fan, X., Li, J., Jia, W., and Peng, P. a.: Technical note: Chemical composition and source identification of fluorescent components in atmospheric water-soluble brown carbon by excitation-emission matrix spectroscopy with parallel factor analysis-potential limitations and applications, Atmospheric Chemistry and Physics, 23, 2613-2625, https://doi.org/10.5194/acp-23-2613-2023, 2023.

Li, P., Yue, S., Yang, X., Liu, D., Zhang, Q., Hu, W., Hou, S., Zhao, W., Ren, H., Li, G., Gao, Y., Deng, J., Xie, Q., Sun, Y., Wang, Z., and Fu, P.: Fluorescence properties and chemical composition of fine particles in the background atmosphere of North China, Advances in Atmospheric Sciences, 40, 1159-1174, https://doi.org/10.1007/s00376-022-2208-x, 2023b.

Comment #9: *L253-256: Use proper significant digits while reporting the numbers throughout the MS. In the number 8436.99, value after decimal (0.99) has no meaning when the SD is also in several thousands.*

Response to Comment #9: We thank the reviewer's kind reminder. We have checked the figures throughout the manuscript and tried to unify the significant digits in the main text and the tables (Table 1 and Table S2). For example, for data greater than 1 (we use the scientific notation for numbers greater than 100), we have uniformly retained three significant digits. As for numbers less than 1, we have kept at most two decimal places. The specific modifications in the main text and tables are as follows,

(1) *"...vary from 2.69 to 19.5 (4.58 ± 0.93-10.1 ± 2.69 on average) and 22.7% to 96.1% (53.4 ± 4.94%-73.3 ± 10.0% on average) across the ten sites..."*

(2) *"As shown in Table 1 and Figure S1, the average Abs_{365} (1.12 ± 0.53-13.1 ± 6.95 Mm^{-1}) and MAE_{365} (0.56 ± 0.11-1.26 ± 0.34 $m^2 \cdot g^{-1}$) of WSOC at the ten sites display significant spatial discrepancies ($p < 0.05$), with HD (SH) has the highest (lowest) average Abs_{365} (13.1 ± 6.95 Mm^{-1} (1.12 ± 0.53 Mm^{-1})) and MAE_{365} (1.26 ± 0.34 $m^2 \cdot g^{-1}$ (0.56 ± 0.11 $m^2 \cdot g^{-1}$)), respectively."*

(3) *"Figure 2 illustrates the average fluorescence volume (FV) and relative contributions of different fluorophores at different sites. Clearly, the average FV of all fluorophores varies in the range of 2.50×10^2-9.76×10^3 RU-nm^2, showing great spatial variability. Overall, the LO-HULIS fluorophore has the highest FV ($1.49\times10^3 \pm 4.74\times10^2$-$9.76\times10^3 \pm 5.82\times10^3$ RU-nm^2 on average) and accounts for the largest proportion (42.2 ± 5.59%-60.3 ± 2.11% on average) in the total fluorophores at most sites (except for TS, NJ and CD), demonstrating the widespread existence of combustion-related sources (especially biomass burning) and their important influence on the fluorophore. In contrast, HO-HULIS fluorophore accounts for the lowest proportion (12.5 ± 1.32%-23.8 ± 2.43% on average, except for TJ and TS). This suggests that the effect of secondary anthropogenic sources at different location may be relatively small during the winter study period. The relatively high FV values of LO-HULIS and non-Nas in northern cities (1.62×10^6 RU-nm^2 in total) compared to southern cities (4.37×10^5 RU-nm^2 in total) and regionals sites (1.76×10^5 RU-nm^2 in total) further indicate the impact of increased primary emissions during the heating season, especially in northern China."*

(4) *"**Table 1.** Light absorption and fluorescence parameters of WSOC measured in this study."*

Sites	Regions	Abs_{365} (Mm^{-1})	MAE_{365} ($m^2 \cdot g^{-1}$)	$AAE_{300-500}$	FI	BIX	HIX
		Avg ± SD	Avg ± SD	Avg ± SD	Avg ± SD	Avg ± SD	Avg ± SD
Tianjin (TJ)	North China	5.57 ± 3.83	0.89 ± 0.22	6.58 ± 0.74	1.48 ± 0.06	0.97 ± 0.06	2.91 ± 0.37
Handan		13.1 ± 6.95	1.26 ± 0.34	5.96 ± 0.36	1.55 ± 0.08	1.00 ± 0.11	1.07 ± 0.43

(HD)							
Qingdao (QD)	*East China*	*4.80 ± 3.09*	*1.03 ± 0.34*	*7.04 ± 0.89*	*1.58 ± 0.09*	*1.08 ± 0.11*	*1.69 ± 0.32*
Nanjing (NJ)		*6.26 ± 3.26*	*0.89 ± 0.25*	*6.66 ± 0.35*	*1.49 ± 0.17*	*0.82 ± 0.12*	*0.56 ± 0.20*
Shanghai (SH)		*1.12 ± 0.53*	*0.56 ± 0.11*	*7.02 ± 0.54*	*1.57 ± 0.09*	*1.02 ± 0.08*	*1.98 ± 0.26*
Xi'an (XA)	*Northwest China*	*10.6 ± 4.42*	*1.04 ± 0.11*	*4.83 ± 1.01*	*1.58 ± 0.08*	*0.96 ± 0.09*	*1.53 ± 0.33*
Chengdu (CD)	*Southwest China*	*5.99 ± 2.61*	*0.65 ± 0.11*	*6.24 ± 0.47*	*1.54 ± 0.10*	*0.80 ± 0.07*	*1.18 ± 0.25*
Chongqing (CQ)		*10.6 ± 4.10*	*0.98 ± 0.09*	*5.78 ± 0.39*	*1.51 ± 0.04*	*0.84 ± 0.04*	*1.37 ± 0.24*
Mt. Tai (TS)	*Regional site*	*2.66 ± 1.22*	*0.74 ± 0.24*	*7.11 ± 0.46*	*1.31 ± 0.17*	*0.75 ± 0.15*	*0.26 ± 0.11*
Heshan (HS)		*3.76 ± 1.55*	*0.64 ± 0.12*	*6.28 ± 0.30*	*1.49 ± 0.03*	*0.77 ± 0.06*	*0.91 ± 0.15*

(5) *"Table S2. Mass concentrations and related ratios of carbonaceous components measured in this study."*

Sites	***Regions***	***OC (μg·m^{-3})***	***EC (μg·m^{-3})***	***WSOC (μg·m^{-3})***	***OC/EC***	***WSOC/OC (%)***	***POC (μg·m^{-3})***	***SOC (μg·m^{-3})***
		Avg ± SD	***Avg ± SD***	***Avg ± SD***	***Avg ± SD***	***Avg ± SD***	***Avg ± SD***	***Avg ± SD***
Tianjin (TJ)	*north China*	*10.0 ± 6.06*	*1.20 ± 0.53*	*5.96 ± 3.21*	*7.99 ± 2.08*	*59.9 ± 11.8*	*5.64 ± 2.47*	*4.38 ± 3.94*
Handan (HD)		*17.9 ± 8.56*	*2.44 ± 0.48*	*10.6 ± 5.33*	*7.06 ± 2.52*	*55.2 ± 13.3*	*8.79 ± 1.72*	*9.08 ± 7.34*
Qingdao (QD)	*east China*	*8.69 ± 5.60*	*1.34 ± 0.83*	*4.68 ± 3.01*	*6.45 ± 1.15*	*55.1 ± 11.6*	*5.86 ± 3.62*	*2.83 ± 2.49*
Nanjing (NJ)		*10.6 ± 4.16*	*2.36 ± 0.83*	*6.82 ± 2.00*	*4.58 ± 0.93*	*65.2 ± 11.9*	*7.03 ± 2.48*	*3.61 ± 2.84*
Shanghai (SH)		*3.31 ± 1.48*	*0.35 ± 0.16*	*1.97 ± 0.83*	*10.1 ± 2.69*	*61.0 ± 6.99*	*1.72 ± 0.79*	*1.59 ± 0.94*
Xi'an (XA)	*northwest China*	*17.8 ± 7.24*	*2.86 ± 1.49*	*10.2 ± 4.55*	*6.90 ± 1.65*	*57.3 ± 6.93*	*12.9 ± 6.74*	*4.87 ± 2.37*
Chengdu (CD)	*southwest China*	*12.2 ± 4.48*	*1.87 ± 0.51*	*8.98 ± 3.09*	*6.44 ± 1.41*	*73.3 ± 10.0*	*6.02 ± 1.63*	*6.17 ± 3.22*
Chongqing (CQ)		*19.6 ± 6.48*	*2.25 ± 0.79*	*10.5 ± 3.45*	*9.02 ± 1.94*	*53.4 ± 4.94*	*13.6 ± 4.78*	*5.96 ± 3.98*
Mt. Tai (TS)	*regional site*	*4.17 ± 2.73*	*0.71 ± 0.74*	*3.60 ± 1.22*	*6.97 ± 3.11*	*65.1 ± 19.6*	*1.91 ± 2.00*	*2.26 ± 1.58*
Heshan (HS)		*9.17 ± 3.54*	*1.38 ± 0.31*	*5.85 ± 2.12*	*6.45 ± 1.52*	*64.4 ± 11.9*	*5.37 ± 1.20*	*3.80 ± 2.55*

Comment #10: *L322-23: What could be possible reasons for such difference?*

Response to Comment #10: We thank the reviewer for the good question and apologize for the insufficient discussion. In the revised manuscript, this paragraph has been rewritten as we have rerun the PMF model, and we

have added the possible reasons for the difference accordingly.

According to the UV-Vis absorption spectra (see the new Figure 4), the WSOC absorption spectra of the ten sites can be roughly divided into two categories: (1) unimodal, that is, the light absorption continues to decline from 250 nm to 700 nm, with a peak around 250 nm; (2) bimodal, that is, there are two significant absorption peaks at around 265 nm and 300 nm. Interestingly, these two types of spectra happen to correspond to the East China sites (i.e., QD, NJ, SH and TS) and the outside East China sites (i.e., TJ, HD, XA, CD, CQ and HS), respectively. Therefore, the WSOC spectra of the two categories were separately put into the PMF model for analysis. In view of the fact that WSOCs at ten sites all have relatively significant light absorption in the range of 250-500 nm, and in order to be consistent with the calculation range of AAE, PMF analysis is carried out for spectra in the band range of 250-500 nm in the revised draft. Therefore, this section has been rewritten in the revised manuscript as follows,

*"**3.2 Identification of light-absorbing substances based on light absorption spectra***

In order to further explore the light absorption characteristics of WSOC and their diversity at different sites, the absorption spectra (250-700 nm) of WSOC are analyzed. Clearly, the light absorption coefficients (Abs_λ) of WSOC at each site exhibit strong wavelength dependence, especially over the UV-visible range (250-500 nm) where there is a significant light absorption signal. According to the UV-visible absorption spectra (see Figure 4), the WSOC absorption spectra measured at the ten sites can be classified into two categories. That is, one type with light absorption continues to decline from 250 nm to 700 nm, with a peak around 250 nm (namely unimodal type), and the other type with two significant absorption peaks at 265 nm and 300 nm (namely bimodal type). Interestingly, these two types of spectra happen to correspond to the sites in East China (unimodal type: QD, NJ, SH and TS) and those outside East China (bimodal type: TJ, HD, XA, CD, CQ and HS), respectively. The differences in the spectral types may be related to differences in the light-absorbing species present in WSOC. Therefore, the PMF-LAS method is further used to analyze the potential categories of the light-absorbing substances. Based on this method, the unimodal and bimodal spectra measured in East China sites and outside East China sites are separately put into the PMF model, and finally three different light absorption factors (namely uni-Fac1, uni-Fac2, uni-Fac3; and bi-Fac1, bi-Fac2, bi-Fac3) are resolved, respectively (see Figure 5 and Figure S11).

By comparing with the light absorption spectra of light-absorbing species in previous studies, the spectra resolved in this study are found to be similar to those of most aromatic or nitrogen-containing heterocyclic compounds. For example, bi-Fac1 exhibits a clear absorption peak at 350 nm and possibly stronger absorption peaks below 250 nm, which is consistent with the spectra of nitro-aromatic compounds such as 4-nitrocatechol (Huang et al., 2021; Lin et al., 2018; Yang et al., 2023). The absorbance of uni-Fac1, uni-Fac2 and bi-Fac2 decreases sharply with increasing wavelength. The uni-Fac2 and bi-Fac2 exhibit an absorption peak at 260 nm, while uni-Fac1 shows no

distinct peaks. These factors are similar to the absorption spectra of nitro-aromatic compounds and nitrogen-free aromatic compounds, respectively (Cao et al., 2023; Jiang et al., 2022a). Additionally, uni-Fac3 and bi-Fac3 have a main absorption peak at around 310 nm and 305 nm, which match the absorption peak of most nitrogen-free aromatic compounds such as vanillin and a few nitro-aromatic compounds or nitrogen-containing heterocyclic compounds (Huang et al., 2021; Li et al., 2020b; Lin et al., 2018; Yang et al., 2023). Taken together, the above spectral analysis suggests that the important light-absorbing components in WSOC may be mainly aromatic compounds or nitrogen-containing compounds. However, it is worth noting that this judgment is based on substances with known absorption spectra, and further studies on more kinds of absorption spectra are needed in the future.

The contributions by different light absorption factors vary significantly at different wavelengths (see Figure S12). For sites locating in East China, the light absorption contribution by uni-Fac1 gradually decreases with the increase of wavelength with the largest contribution at 250 nm. In contrast, the absorption contribution of uni-Fac3 increases significantly over 250-325 nm and then slowly over 325-500 nm. The absorption contribution of uni-Fac2 decreases first and then increases, with the minimum contribution appearing around 340 nm. For sites in outside East China, the contribution of bi-Fac1 is relatively stable in the 250-300 nm range, but increases significantly with wavelength at the wavelengths above 300 nm. In contrast, the proportional contribution of bi-Fac2 is similar to that of uni-Fac1, which monotonically decreases with increasing wavelength throughout the entire spectral range (250-500 nm). The proportional contribution of bi-Fac3 significantly increases in the range of 250-320 nm, and then remains stable or slightly decreases thereafter. Overall, uni-Fac1 is the main absorption factor at sites in East China, while bi-Fac3 is the major absorption factor at sites outside East China, contributing to 38.9 ± 10.4%-53.5 ± 13.5% and 39.5 ± 22.7%-51.1 ± 20.0% (on average) of the total light absorption, respectively. This suggests that nitro-aromatic or nitrogen-free aromatic compounds with strong wavelength dependence are the main light-absorbing species in WSOC at the ten sites, highlighting the importance of aromatic structure to WSOC light absorption. However, it is worth noting that this is only preliminary knowledge based on substances with known absorption spectra. The three types of light-absorbing factors may contain different aromatic and other light-absorbing substances, which may have different relative contributions, and therefore present significantly different light absorption spectra. In the future, it is necessary to combine mass spectrometry techniques to explore the composition of light-absorbing substances in different classes at the molecular level."

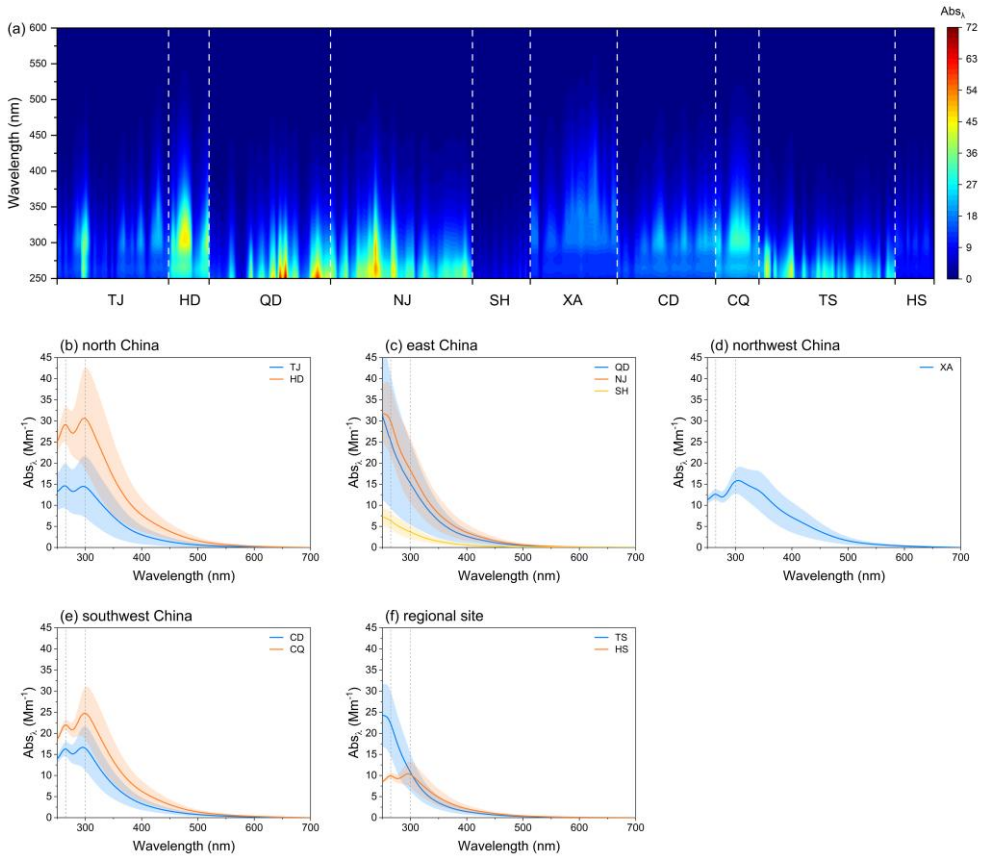

Figure 4. *(a) Light absorption coefficient spectrum of WSOC at each site and the average light absorption spectrum in (b) north China, (c) east China, (d) northwest China, (e) southwest China, and (f) regional sites. Note: The color bar represents the magnitude of the Abs$_\lambda$.*

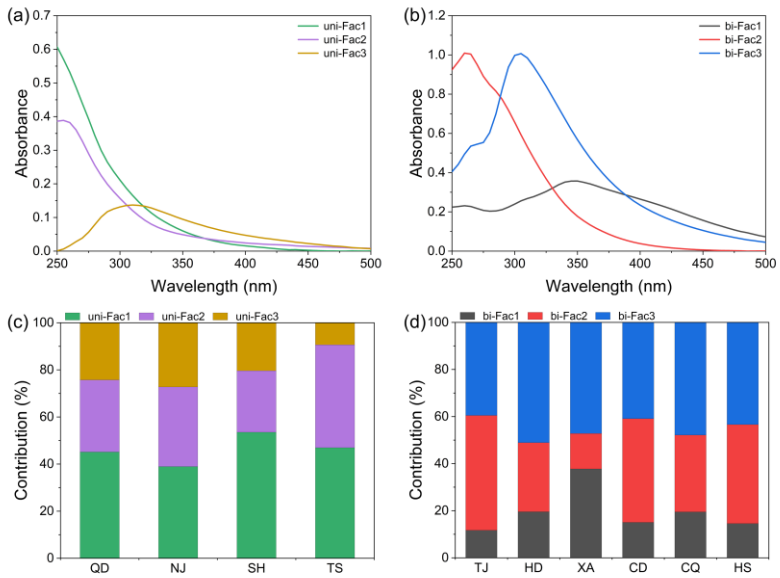

Figure 5. *The average light absorption spectra of the absorption factors resolved by PMF model at (a) East China sites (unimodal absorption spectral type) and (b) outside East China sites (bimodal absorption spectral type), as well as the average contribution by each factor calculated according to the integral absorbance from 250-500 nm*

at both types of sites (panel c and d).

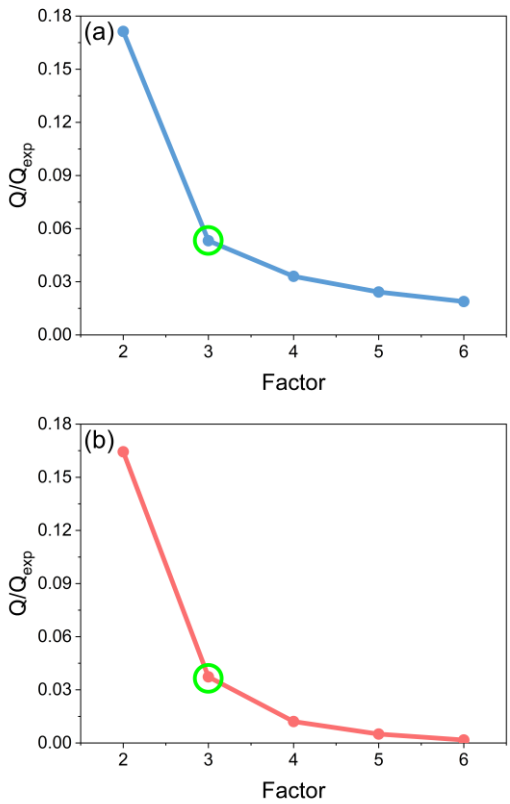

Figure S11. *The $Q/Q_{expected}$ ratios of different factors resolved by PMF model at (a) East China sites (unimodal absorption spectral type) and (b) outside East China sites (bimodal absorption spectral type)*

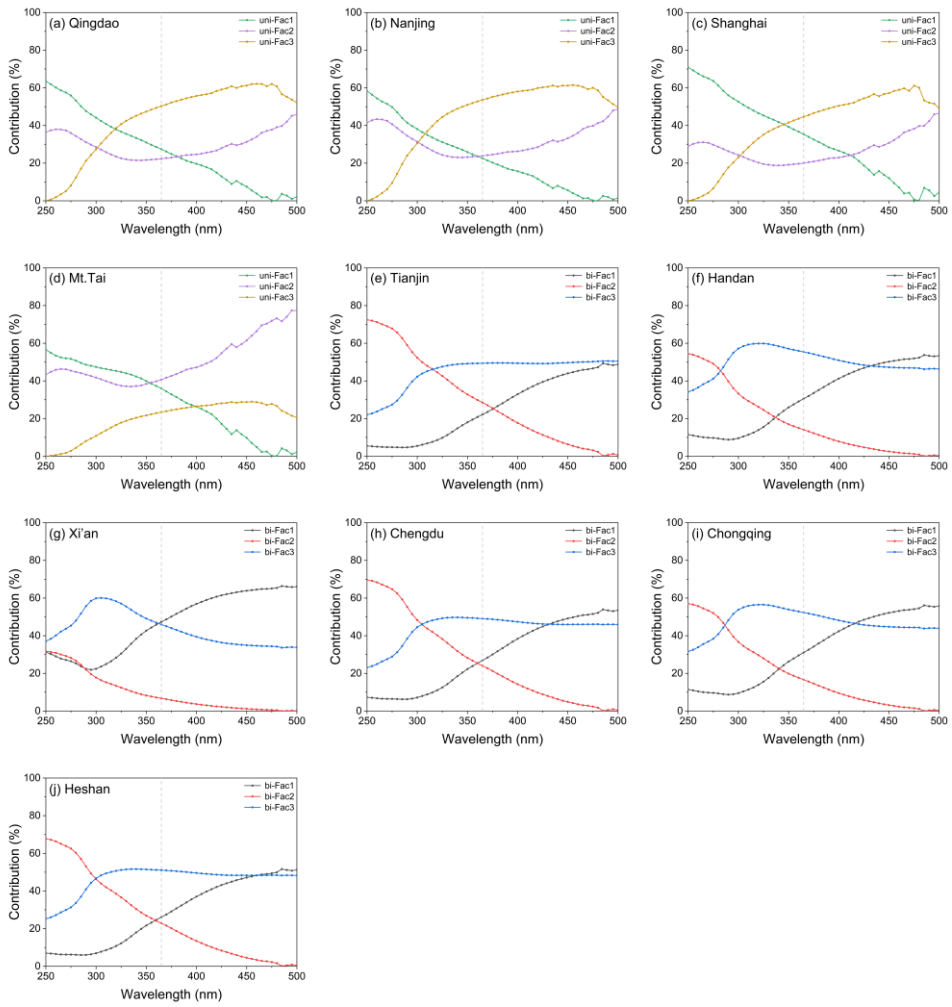

Figure S12. *The proportional contributions of different factors at different wavelengths at (a-d) East China sites and (e-j) outside East China sites. Note: The dotted line represents the position of 365 nm.*

<u>Comment #11:</u> *L335-343: Such discussions shall be supported by some other independently measured species. Otherwise, it will be considered as hypothetical statement.*

<u>Response to Comment #11:</u> We thank the reviewer's kind reminder and constructive suggestion. Combining with the **Comment #12**, we have rewritten this section in the manuscript as follows,

"To investigate the influence of air quality levels on the light absorption properties of WSOC, the sampling days are classified into five pollution levels including clean (0-35 μg·m^{-3}), relatively clean (35-75 μg·m^{-3}), slightly polluted (75-115 μg·m^{-3}), moderately polluted (115-150 μg·m^{-3}), and heavily polluted (> 150 μg·m^{-3}) according to the national ambient air quality daily Grade-II standard threshold values and ambient air quality indices. <u>As shown in Figure 7a and b, Abs_{365} and MAE_{365} of WSOC both increase with the increase of pollution levels, in which Abs_{365} changes significantly ($p < 0.01$) while MAE_{365} changes relatively gently. The enhancement of WSOC light</u>

absorption under high pollution conditions may be related to the increase of WSOC concentration, light absorption capacity and light-absorbing species. Previous studies have reported that the mass fractions of oxidized organic aerosols increase significantly with the increase of $PM_{2.5}$ mass concentration, and the oxidized organic aerosols contain a large number of light-absorbing species such as nitroaromatics compounds (You et al., 2024). In this study, the relative abundances of O-H, C=C and R-ONO_2 functional groups, which are related to aromatic compounds and have a good positive correlation with the light absorption of WSOC, increase with $PM_{2.5}$ mass concentration (see Figure S14, and discussion in the next section). Additionally, the accumulation of anthropogenic emissions (especially those sources with strong light-absorbing BrC such as biomass burning and coal combustion sources) at high pollution levels will lead to an increase in BrC chromophore types and overall light absorption capacity (Li et al., 2020a; Tang et al., 2020; Wei et al., 2020).”

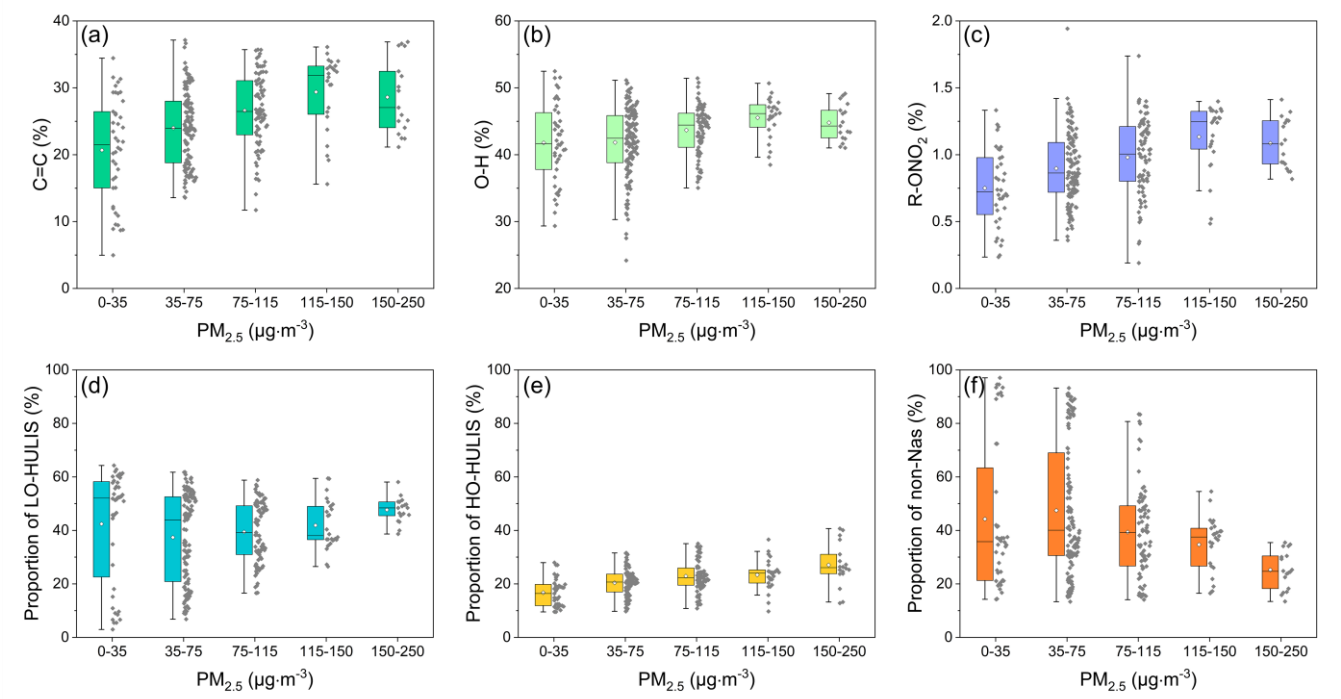

Figure S14. *Variations of the relative abundance of functional groups (a) C=C, (b) O-H and (c) R-ONO_2 and the proportion of (d) LO-HULIS, (e) HO-HULIS and (f) non-Nas fluorophores with $PM_{2.5}$ mass concentrations.*

References:

Li, J. J., Zhang, Q., Wang, G. H., Li, J., Wu, C., Liu, L., Wang, J. Y., Jiang, W. Q., Li, L. J., Ho, K. F., and Cao, J. J.: Optical properties and molecular compositions of water-soluble and water-insoluble brown carbon (BrC) aerosols in northwest China, Atmospheric Chemistry and Physics, 20, 4889-4904, https://doi.org/10.5194/acp-20-4889-2020, 2020a.

Tang, J., Li, J., Su, T., Han, Y., Mo, Y. Z., Jiang, H. X., Cui, M., Jiang, B., Chen, Y. J., Tang, J. H., Song, J. Z., Peng,

P. A., and Zhang, G.: Molecular compositions and optical properties of dissolved brown carbon in biomass burning, coal combustion, and vehicle emission aerosols illuminated by excitation-emission matrix spectroscopy and Fourier transform ion cyclotron resonance mass spectrometry analysis, Atmospheric Chemistry and Physics, 20, 2513-2532, https://doi.org/10.5194/acp-20-2513-2020, 2020.

Wei, Y., Chen, H., Sun, H., Zhang, F., Shang, X., Yao, L., Zheng, H., Li, Q., and Chen, J.: Nocturnal $PM_{2.5}$ explosive growth dominates severe haze in the rural North China Plain, Atmospheric Research, 242, https://doi.org/10.1016/j.atmosres.2020.105020, 2020.

You, B., Zhang, Z., Du, A., Li, Y., Sun, J., Li, Z., Chen, C., Zhou, W., Xu, W., Lei, L., Fu, P., Hou, S., Li, P., and Sun, Y.: Seasonal characterization of chemical and optical properties of water-soluble organic aerosol in Beijing, Science of The Total Environment, 930, 172508, https://doi.org/10.1016/j.scitotenv.2024.172508, 2024.

Comment #12: *L345-346: It looks a wrong statement. The mentioned processes make the light absorption properties of BrC variable, as reported in numerous studies.*

Response to Comment #12: We apologize for the misleading. Taking into account the **Comment #11** by the reviewer, we have rewritten this section. Please refer to the **Response to Comment #11**.

Comment #13: *L350-351: This statement looks counter intuitive.*

Response to Comment #13: We thank the reviewer for pointing this out. Combining with the **Comment #14**, we have revised this statement in the revised manuscript as follows,

"The fluorescence volumes normalized (NFV) by WSOC concentration of different fluorophores exhibit different variation trends with $PM_{2.5}$ mass concentrations (see Figure 7c-e). Overall, the total NFV value of HULIS increases with $PM_{2.5}$ concentrations, with the increase of HO-HULIS being more monotonous and significant ($p < 0.01$, based on Spearman's rank correlation test) while the increase of NFV of LO-HULIS being less significant ($p > 0.05$). In contrast, the NFV of non-Nas fluorophore decreases with the increase of $PM_{2.5}$ concentrations. This suggests that HO-HULIS is the dominant fluorophore under contaminated conditions (see Figure S14). The different degrees of increase in HO-HULIS and LO-HULIS highlight the contributions of combustion related sources and secondary sources and the increase of aerosol oxidation under high pollution levels. This also implies an increase in chromophores with aromatic or heterocyclic structures under pollution conditions, which is consistent with the indication of functional groups."

References:

Li, P., Yue, S., Yang, X., Liu, D., Zhang, Q., Hu, W., Hou, S., Zhao, W., Ren, H., Li, G., Gao, Y., Deng, J., Xie, Q., Sun, Y., Wang, Z., and Fu, P.: Fluorescence properties and chemical composition of fine particles in the background atmosphere of North China, Advances in Atmospheric Sciences, 40, 1159-1174, https://doi.org/10.1007/s00376-022-2208-x, 2023.

Comment #14: *L352-353: self-contradictory statement!*

Response to Comment #14: We are sorry for the self-contradictory statement. We have revised the statement in this paragraph in the revised manuscript. Please refer to the **Response to Comment #13** for the specific modifications.

Minor Comments:

Comment #15: *L158-160: It looks odd. One can simply refer the figure and come to the discussion point.*

Response to Comment #15: We thank the reviewer for pointing this out. These sentences have been modified as follows in the revised manuscript,

"During the observation period, the mass concentrations of carbonaceous components (i.e., OC, EC and WSOC) increase with the increase of $PM_{2.5}$ concentration (see Figure S3), and exhibit significant spatial variations across the ten sites ($p < 0.05$). As shown in Figure S1 and Table S2, the average concentrations of OC, EC and WSOC observed at the ten sites ranged from 3.31 to 19.6 $\mu g \cdot m^{-3}$, 0.35 to 2.86 $\mu g \cdot m^{-3}$, and 1.97 to 10.6 $\mu g \cdot m^{-3}$, respectively, with the highest mean mass concentrations of OC, EC and WSOC observed in CQ, XA, and HD, respectively, while the lowest values all observed in SH. Overall, the regional average carbonaceous component concentrations show the spatial distribution trends of northwest China > southwest China > north China > east China > regional site ($p < 0.05$)."

Comment #16: *Fig. 2: For similar Log (MAE_{405}), there is a considerable variability in AAE. Explain this observation.*

Response to Comment #16: We thank the reviewer for pointing this out. This may be due to the following reasons:

(1) The variation ranges of MAE_{405} were missing in the original Figure 2. This means that the different AAE values

may not correspond to the same or similar MAE values.

(2) AAE value is mostly influenced by particle size, and the optical properties of light-absorbing substances and the coatings, and it may also significantly depend on the extraction method (degree of dilution) (Zhang et al., 2013). The different extraction methods used in different studies may be also a reason for the variability in AAE values.

(3) AAE is commonly used to represent the wavelength dependence of BrC light absorption within a certain wavelength range, while MAE represents the light absorption capacity per unit mass of BrC, which is usually calculated by selecting a single wavelength (e.g., 365 nm, 405 nm). Therefore, AAE, which presents the light absorption characteristics of BrC within a certain wavelength range, theoretically has no fixed negative or positive relationship with MAE value calculated based on a single wavelength. In some cases, similar MAE values for BrC calculated at the same wavelength may correspond to different AAE values. For example, the MAE_{405} of sample A and B in this study are almost identical, but the $AAE_{300\text{-}500}$ of sample B is significantly lower than that of sample A, because the spectra of the two samples were different (see Figure R2).

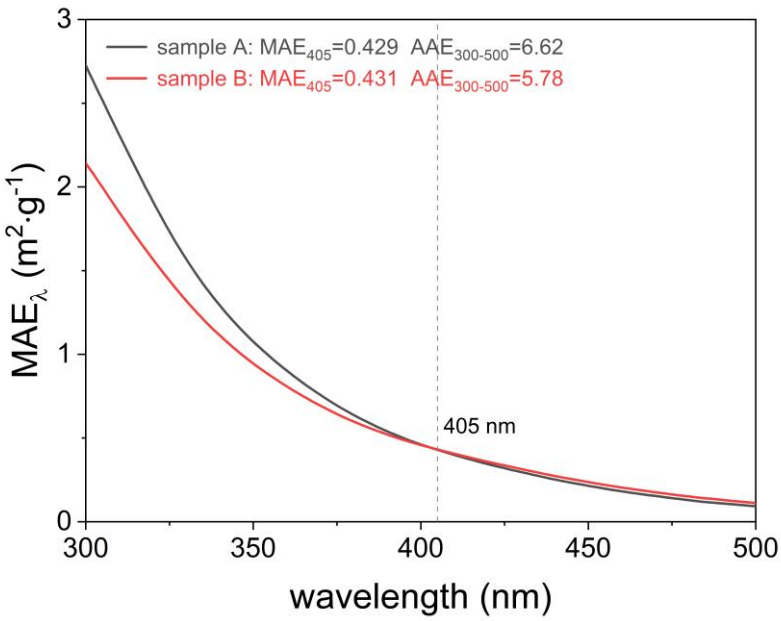

Figure R2. The MAE spectra of sample A and sample B within the range of 300-500 nm. Note: The dashed line represents the position of 405 nm.

In the revised manuscript, the original Figure 2 (presented as new Figure 1) has been replotted by adding the variation range of MAE_{405} values for the samples measured in this study, and the AAE values were recalculated within the range of 300-500 nm ($AAE_{300\text{-}500}$).

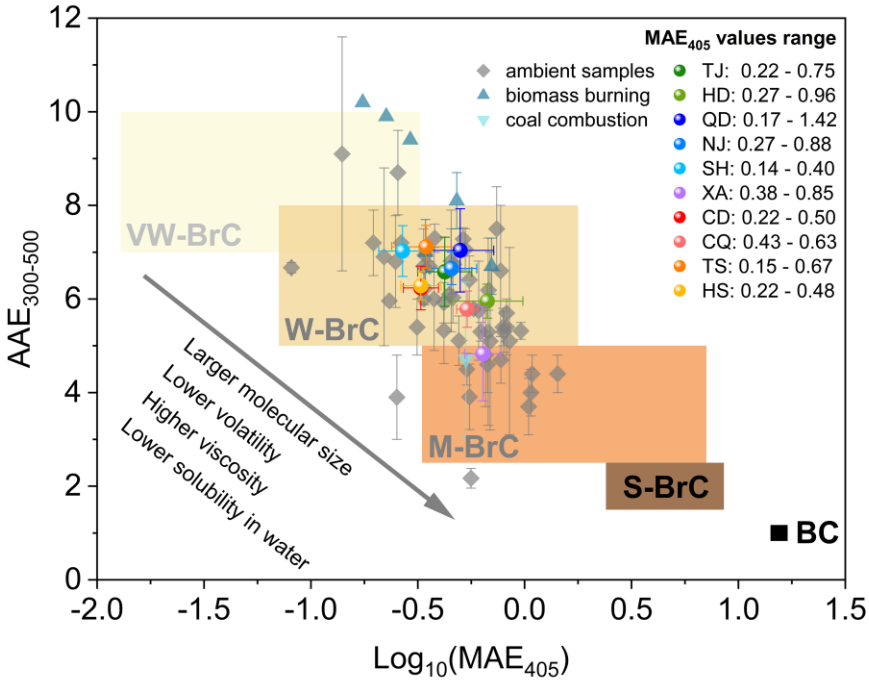

Figure 1. *Graphical representation of optical-based BrC classes in $log_{10}(MAE_{405})$-AAE space. The shaded regions represent very weakly light-absorbing BrC (VW-BrC), weakly light-absorbing BrC (W-BrC), moderately light-absorbing BrC (M-BrC), strongly light-absorbing BrC (S-BrC), and absorbing BC, respectively.*

References:

Zhang, X., Lin, Y., Surratt, J., Weber, R.: Sources, composition and absorption Ångström exponent of light-absorbing organic components in aerosol extracts from the Los Angeles Basin. Environmental Science & Technology, 47, 3685-3693, https://pubs.acs.org/doi/10.1021/es305047b, 2013.

Comment #17: *Fig. 3: Explain legends and add what is represented by grey region?*

Response to Comment #17: We apologize for the confusion. In the original Figure 3, the legend shows the categories of fluorophores represented by different colors. For example, blue denotes LO-HULIS, yellow denotes HO-HULIS, and orange denotes non-Nas, respectively. The bar chart shows the absolute FV value of each fluorophore and the pie chart show the relative proportion of each fluorophore. While the gray region in the pie chart is only served as the background color for this type of circular graph and has no practical significance. The purpose of adding the gray region here is to see more clearly that there are three parallel components in total (Therefore, three circles can be seen).

In order to avoid ambiguity, in the new Figure 2, we deleted the gray background in the pie chart and modified the

title as follows:

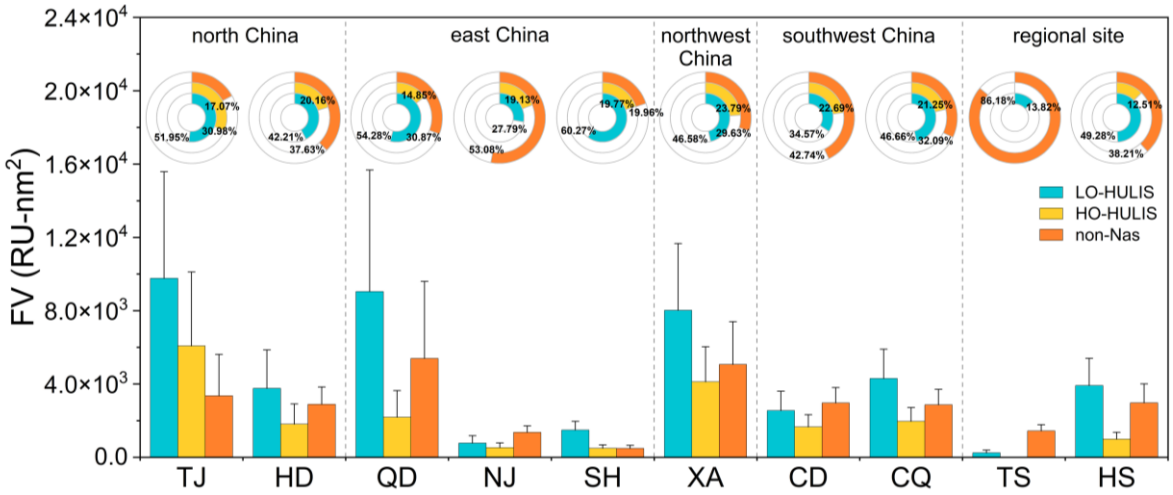

*"**Figure 2.** The absolute fluorescence volumes (bar chart) and fractional contributions (pie chart) of each fluorophore at different observation sites. Note: Blue denotes LO-HULIS, yellow denotes HO-HULIS, and orange denotes non-Nas."*

Comment #18: *Fig. 4: There are multiple peaks within different bands. Can't they be identified and added here?*

Response to Comment #18: We agree with the reviewer that it would be good to identify or even quantify more peaks. Unfortunately, in this study, we did not use standard materials to explore new functional group peaks, but only identified them on the basis of previous studies.

Many functional groups in WSOC have been identified in previous studies. However, due to the complexity of BrC structure and possible measurement bias, the spectral peak position of the same type of functional group may not be exactly consistent across different studies, but rather within a certain wavelength band. For example, the two small peaks within the range of 1220-1510 cm^{-1} in this study have been both identified as the C=C bond in previous studies, and the small peaks within the range of 2635-3600 cm^{-1} in this study are all related to the O-H bonds (Fan et al., 2023; Coury and Dillner, 2008; Wang et al., 2023; Yang et al., 2024). Furthermore, some small sharp peaks, such as one in the range of 977-1220 cm^{-1} in this study, may be caused by noise interference during the measurement process, so we did not define these peaks separately. Therefore, we treated the peaks with obvious signal/noise ratio in a certain region as a class of functional groups, and ignored some small peaks that may be disturbed by noise, which is consistent with the broader definition in previous studies (Fan et al., 2023; Wang et al., 2021). More tests combined with standard substances (especially known BrC species) are needed in the future to accurately identify more functional group peaks.

References:

Coury, C. and Dillner, A. M.: A method to quantify organic functional groups and inorganic compounds in ambient aerosols using attenuated total reflectance FTIR spectroscopy and multivariate chemometric techniques, Atmospheric Environment, 42, 5923-5932, https://doi.org/10.1016/j.atmosenv.2008.03.026, 2008.

Fan, X., Cheng, A., Chen, D., Cao, T., Ji, W., Song, J., and Peng, P.: Investigating the molecular weight distribution of atmospheric water-soluble brown carbon using high-performance size exclusion chromatography coupled with diode array and fluorescence detectors, Chemosphere, 338, 139517, https://doi.org/10.1016/j.chemosphere.2023.139517, 2023.

Wang, D., Yang, X., Lu, H., Li, D., Xu, H., Luo, Y., Sun, J., Hang Ho, S. S., and Shen, Z.: Oxidative potential of atmospheric brown carbon in six Chinese megacities: Seasonal variation and source apportionment, Atmospheric Environment, 309, https://doi.org/10.1016/j.atmosenv.2023.119909, 2023.

Wang, X., Qin, Y., Qin, J., Long, X., Qi, T., Chen, R., Xiao, K., and Tan, J.: Spectroscopic insight into the pH-dependent interactions between atmospheric heavy metals (Cu and Zn) and water-soluble organic compounds in $PM_{2.5}$, Science of the Total Environment, 767, 145261, https://doi.org/10.1016/j.scitotenv.2021.145261, 2021.

Yang, X., Huang, S., Li, D., Xu, H., Zeng, Y., Yang, L., Wang, D., Zhang, N., Cao, J., and Shen, Z.: Water-soluble organic matter with various polarities in $PM_{2.5}$ over Xi'an, China: Abundance, functional groups, and light absorption, Particuology, 84, 281-289, https://doi.org/10.1016/j.partic.2023.07.005, 2024.